Coordination Chemistry Reviews 255 (2011) 2653–2665

Contents lists available at ScienceDirect

Coordination Chemistry Reviews

journal homepage: www.elsevier.com/locate/ccr

Review

Harvesting luminescence via harnessing the photophysical properties of transition metal complexes

Pi-Tai Chou[a,*], Yun Chi[b,**], Min-Wen Chung[a], Chao-Chen Lin[a]

[a] Department of Chemistry, National Taiwan University, No. 1, Sec. 4, Roosevelt Road, Taipei 10617, Taiwan, ROC
[b] Department of Chemistry, National Tsing Hua University, No. 101, Sec. 2, Kuang-Fu Road, Hsinchu 30013, Taiwan, ROC

Contents

ARTICLE INFO

Article history:
Received 30 September 2010
Accepted 10 December 2010
Available online 21 December 2010

Keywords:
Transition metal complex
Spin–orbit coupling
Intersystem crossing
Phosphorescence
Metal-centred *dd* transition
Metal-to-ligand charge transfer

ABSTRACT

The main goal of this review is to provide systematic elucidation of the correlation between structural characters and the photophysical properties of a series of heavy transition metal complexes. Depending on types of metal ions, chromophoric and ancillary ligands, several intriguing cases encountered in our recent studies will be exemplified as prototypes to shed light on their excited-state relaxation pathways. Particular attention is paid to: (i) the intersystem crossing and/or radiative decay rates versus contribution of the metal d_π orbital, (ii) crucial factors that facilitate the radiationless deactivation, such as the metal-centred *dd* transition, resulting in weakness of the metal–ligand bond, and other transitions weakening the specific bonds and flexible structural framework that induces the low-frequency vibrational deactivation, (iii) intra-ligand versus inter-ligand charge transfer affecting the photophysical properties; that is, an issue of current interest regarding whether to treat the whole transition metal complex as a single entity or as several distinctive chromophores separated by the core metal ion. We then formulate a discussion from the standpoint of fundamental photophysical theory. The results, together with modern computational approaches for supplementary support, allow us to make adequate comparison with respect to classic organic fluorescence counterparts. Many similarities can be identified between organic fluorophores and late transition metal based phosphors; nevertheless, certain distinctions can also be extracted. We then conclude this review by providing guidelines on how to harvest the emission via suppressing the weighting of radiationless deactivation routes. However, for transition metal complexes, quantitative assessment of radiationless deactivation and hence the accurate prediction of emission efficiency is still a long term goal to be attained.

1. Introduction

Luminescent transition-metal complexes constitute an important class of materials that have attracted intensive attention during the past two decades. Thousands of compounds have been

* Corresponding author. Tel.: +886 2 3366 3894; fax: +886 2 2369 5208.
** Corresponding author. Tel.: +886 3 571 2956; fax: +886 3 572 0864.
E-mail addresses: chop@ntu.edu.tw (P.-T. Chou), ychi@mx.nthu.edu.tw (Y. Chi).

0010-8545/$ – see front matter © 2010 Elsevier B.V. All rights reserved.
doi:10.1016/j.ccr.2010.12.013

synthesized and extensive research has been reported on their fundamentals such as synthetic strategies, and the associated chemistry, photophysics and photochemistry. This incentive is apparently driven by the heavy atom enhanced spin–orbit coupling, giving partial mixing between triplet and singlet manifolds. The consequence gives rise to fast rate of intersystem crossing and hence highly efficient population in the lowest lying triplet state (T_1), followed by phosphorescence perhaps with high yield. This niche has made emitting transition metal complexes very promising for a wide range of applications. Of particular importance are the promising applications in optoelectronics such as organic light-emitting diodes (OLEDs) and photovoltaics. As for OLEDs, upon charge recombination, theoretical unity efficiency can be reached for late transition metal complexes, rather than the maximum of 25% for the classic fluorescent organic counterparts.

In developing strategies for the design and synthesis of luminescent transition metal complexes, it is of key importance to select both chromophoric and ancillary chelates with appropriate photophysical characteristics. From the fundamental point of view, one of the top priorities is to develop detailed understanding of the various factors that govern the basic photophysical behaviors. This can be ascertained by various sophisticated spectroscopic techniques together with theoretical approaches; the results thus acquaint synthetic chemists with the knowledge of electronic transitions as well as dynamics of relaxation that occur between different states associated with central metal atom and surrounding ligands, facilitating further improvement and route to the designated application.

With respect to the ligand chromophores, cyclometalated aromatics have been commonly used for assembling such luminescent metal compounds [1–10]. Recently, 2-pyridyl azolate and its functionalized analogues have emerged as popular alternatives for the design of more advanced luminescent materials [11–14]. These successes are mainly attributed to their rigid coordination framework and robust metal–ligand bonding interaction, which in turn increases the $d_\pi \rightarrow d_{\sigma^*}$ (*dd*) energy gap and hence affords far less radiationless quenching due to the suppressed thermal population of this metal-centred transition possessing repulsive potential energy surface (PES). This is particularly true for the third-row late transition-metal elements [15], which possess a large ligand field that further destabilizes the *dd* state. Certainly, the repulsive *dd* state cannot be the sole deactivation channel in the transition metal complexes. Quenching of emission induced by other deactivation pathways such as structural deformation, low frequency, high density rotation and specific bond weakening to raise shallow PES, etc. also play crucial roles. We will present in-depth discussion on the relevant issue in the following sections.

In addition to the above mentioned metal-centred *dd* state, three basic transition processes are commonly encountered, namely the metal-to-ligand charge transfer transition (MLCT), ligand-centred (LC) $\pi\pi^*$, and ligand-to-ligand charge transfer (LLCT) in the singlet manifold [16–19]. The last term proceeds from the occupied molecular orbitals of one type of ligand to the unoccupied molecular orbitals of other ligands. Confirmation of LLCT transitions is commonly hampered by the co-existence of other isoenergetic processes, such as *dd*, MLCT and LC $\pi\pi^*$ transitions. Nevertheless, for LLCT, the relocation of electron density across different ligands may be associated with large changes in dipole moment [20,21]. As a result, the contribution from LLCT transition in the lowest lying excited state of luminescent transition metal complexes may be manifested by the associated solvent polarity dependent phosphorescence. The mixing of close-lying, metal-to-ligand charge transfer transition (MLCT) and ligand-centred (LC) $\pi\pi^*$ electronic transitions makes the fast singlet-to-triplet intersystem crossing feasible. The net result is to increase the transition probability, hence shortening the radiative lifetime of the observed photoluminescence.

This collaborative research group has long been intrigued by the photoluminescence of late transition metal complexes [2,11–13]. After lengthy endeavors, we have undertaken the systematic study of their electronic transitions and explored correlations of the photophysical properties versus various lower lying electronic excited states. Like their organic fluorescent counterparts, the luminescent behavior of these late transition metal complexes can be interpreted by the use of fundamental photophysics and modern molecular orbital theory. For the luminescent complexes assembled, employing both chromophoric and ancillary ligands, it has been found that the electron density in each of the frontier molecular orbitals is not evenly distributed, but preferentially located at the metal centre and/or chromophoric ligands, where tuning of emission wavelength and other photophysical properties can be executed by judiciously altering the chemical subtlety on each fragment. The electronic transition can thus be considered as the one-electron excitation that occurs among various associated frontier orbitals. This makes design and synthesis of luminescent complexes feasible if one can gain detailed understanding of the specific factors that control the basic photophysical properties. In this review, we describe the intrinsic properties of the excited states in selected systems encountered in our recent advances. The majority contain a late transition metal atom, which is further coordinated by a range of cyclometalating chelates, including 2-pyridyl azolate and its functionalized analogues.

The following sections are organized according to a sequence of steps, wherein we first address the unique properties of the transition metal complex to enhance spin–orbit coupling and its role in relaxation dynamics. The next step involves presentation of the photophysics of several paradigms that can serve as prototypes to elucidate their unique photophysical properties. Particular attention is paid to intersystem crossing and/or radiative decay rates versus contribution of the metal d_π orbital, crucial factors such as the metal-centred *dd* state, the weakness of specific bonds and flexible structural framework, etc. to facilitate radiationless transition. Here, common phenomena such as O_2 collisional quenching and triplet–triplet annihilation are excluded upon dealing with the radiationless deactivation pathways of the triplet state. In solution, the former and the latter quenching processes can be avoided by degassing and lowering the triplet-state concentration, respectively. Also, both processes are negligible in solid due to the much slower diffusion rate, unless a very high triplet-state concentration is prepared for the latter case, a phenomenon commonly encountered in OLEDs upon operation at higher driving voltage [22]. Finally, with the assistance of theoretical approaches, attempts have also been made to provide guidance for the readership regarding relaxation pathways versus variation of metal ions, chromophoric and ancillary chelates.

2. Factors governing harvest of phosphorescence

2.1. Population to the lowest lying triplet state

Two gross criteria are essential if one intends to attain highly emissive phosphorescence; (a) high $S_1 \rightarrow T_n$ intersystem crossing (ISC) efficiency and (b) much less competitive radiationless deactivation with respect to $T_1 \rightarrow S_0$ radiative transition. The former implies that the rate of $S_1 \rightarrow T_n$ intersystem crossing should be so fast that it ideally would surpass all other $S_1 \rightarrow S_0$ recovery processes to achieve unity population in the triplet manifold. To simplify the approach, we assume that the intersystem crossing takes place solely via the $S_1 \rightarrow T_1$ pathway. The corresponding rate

constant, k_{isc}, is then expressed as:

$$k_{isc} \propto \frac{< \psi_{T_1} \left| H_{so} \right| \psi_{S_1} >^2}{(\Delta E_{S_1-T_1})^2} \quad (1)$$

where H_{so} is the Hamiltonian for spin–orbit coupling (SOC) and $\Delta E_{S_1-T_1}$ is the energy difference between S_1 and T_1 states. An oversimplified approach taking Os(II) ion as a hydrogen-like atom deduces k_{isc} to be proportional to Z^8/r^6, where Z stands for the atomic number and r is the distance between the metal atom and the centre of chromophore involved in the transition [23]. Since the metal d_π orbital is directly coupled into the spin–orbit coupling matrix, the rate of $S_1 \rightarrow T_1$ intersystem crossing should be greatly influenced as well as enhanced by those low lying transitions incorporating a metal d_π orbital. Moreover, mixing of MLCT and $\pi\pi^*$ in both S_1 and T_1 states leads to an $S_1 \rightarrow T_1$ intersystem crossing process incorporating $<^1 d_\pi \pi^* | H_{so} |^3 \pi\pi^*>$ or $<^3 d_\pi \pi^* | H_{so} |^1 \pi\pi^*>$ terms. The combination of these two factors induces changes of orbital angular momentum, i.e. $d_\pi \rightarrow \pi$ or vice versa, which may effectively couple with the flip of electron spin. As a result, the transition has a significantly large first-order spin–orbit coupling term, and the rate of intersystem crossing would be greatly enhanced [24]. Conversely, for the $S_1 \rightarrow T_1$ intersystem crossing involving pure $\pi\pi^*$ (either ILCT or LLCT) character only, the core metal ion may be empirically treated as an element that virtually executes an external heavy atom effect. For this case, the distance (r) between emitting chromophore and metal centre becomes critical due to the empirical inverse r^6 proportionality for the heavy atom effect [13].

The above concept of metal d_π orbital and distance tuning $S_1 \rightarrow T_1$ ISC was recently demonstrated via a series of β-diketonate Os(II) complexes with formulae $[Os(CO)_3(tfa)(L\hat{}X)]$ (**1**–**7**), which were synthesized from the Os(I) dimer $[Os_2(CO)_6(tfa)_2]$ (tfa = trifluoroacetate) with respective diketone reagents (L^X)H in a Carius tube or autoclave via the mechanism of $Os_2(CO)_6(tfa)_2 + (L\hat{}X)H \rightarrow [Os(CO)_3(tfa)(L\hat{}X)] + H_2$ [25]. The structures of these complexes and their systematically varying photophysical properties are summarized in Fig. 1. From the viewpoint of steady-state spectroscopy, complexes **1** and **2** exhibit solely the phosphorescence with peak wavelength at 545 nm and 520 nm, respectively. Upon further substitution with either α or β-naphthalene, forming **3** and **4**, dual emission consisting of both fluorescence and phosphorescence is resolved. The appearance of fluorescence, though being the minor component in intensity, indicates their reduced $S_1 \rightarrow T_1$ intersystem crossing rate. For complex **5**, bearing a pendant 2-anthracene moiety, dual emission consisting of fluorescence (550 nm) and phosphorescence (690 nm) with nearly equal intensity is observed in degassed solution. In sharp contrast, complex **6**, with 1-pyrene as the substituent, exhibits fluorescence only.

The above steady-state description correlates well with the time-resolved measurement, in which the rate constant of ISC, monitored by the decay rate constant of the fluorescence (assuming decay of the S_1 state to be dominated by ISC), decreases in the order of **1** (150 fs)$^{-1}$ > **2** (480 fs)$^{-1}$ > **3** (3.64 ps)$^{-1}$ > **4** (6.71 ps)$^{-1}$ > **5** (120 ps)$^{-1}$ ≫ **6** (2.1 ns)$^{-1}$ (see Fig. 1) [26,27]. Also, in a qualitative manner, the trend of k_{isc} ($S_1 \rightarrow T_1$) can be rationalized by the percentage of MLCT involved and hence the degree of mixing between MLCT and $\pi\pi^*$ in both S_1 and T_1 manifolds. The greatest MLCT% (in S_1, see Fig. 1) character in **1** gives rise to ultrafast system response limited k_{isc} (>10^{13} s^{-1}). As for the lack of MLCT/$\pi\pi^*$ mixing in **5**, k_{isc} decreases drastically to ~9.2×10^9 s^{-1}, a reduction of more than three orders of magnitude (c.f. **1**). Due to the lack of MLCT contribution, complexes **5** and **6** mainly undergo $^1\pi\pi^* \rightarrow {}^3\pi\pi^*$ intersystem crossing, for which the coupling between orbital and spin angular momentum, or $<^1\pi\pi^* | H_{so} {}^3\pi\pi^*>$, should be rather small because of negligible changes in orbital angular momentum

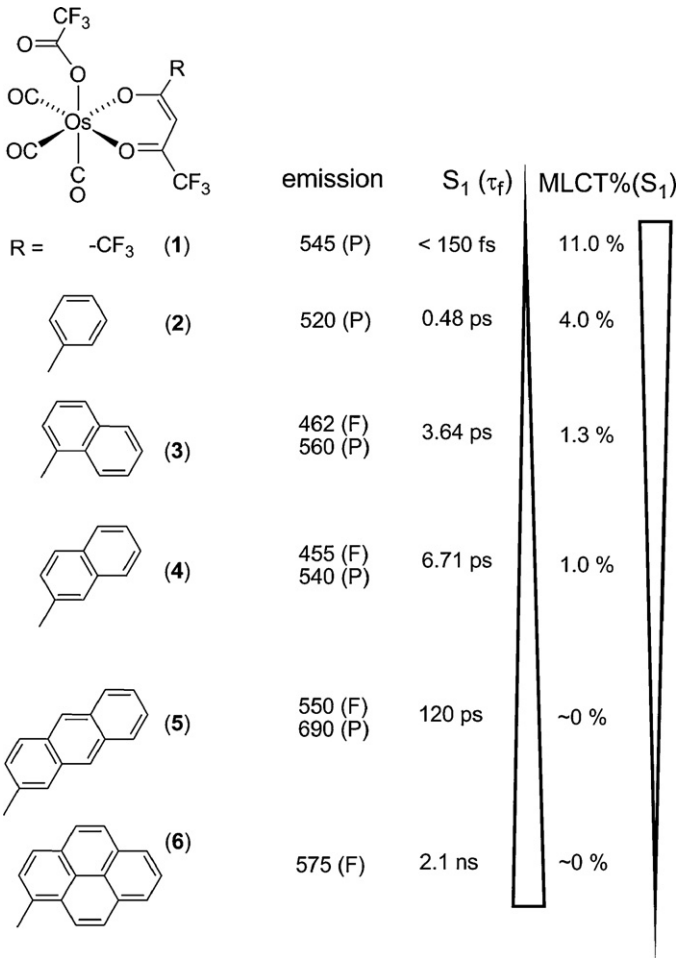

Fig. 1. Structures and photophysical properties (in CH_2Cl_2) of Os(II) metal complexes **1**–**6** bearing β-diketonate ligands with differing π-conjugation. Parenthesis: F and P denote fluorescence and phosphorescence, respectively.

that can be coupled to the spin flipping. In other words, there is little first-order spin–orbit coupling to enhance the $S_1 \rightarrow T_1$ ISC process. For this case, the core Os(II) atom can be virtually treated as an external heavy atom. The much slower rate (<(2.1 ns)$^{-1}$) of ISC in **6** shows the distance r (and hence $1/r^6$) from the Os(II) atom to the centre of gravity of the aromatic pendants to be crucial, which is calculated to be 6.17 Å and 7.89 Å for **5** and **6**, respectively.

The above series of Os(II) complexes provide a paradigm for comprehensive studies of the rate of $S_1 \rightarrow T_1$ ISC versus structure (electronic configuration). An ultrafast rate constant (>(1 ps)$^{-1}$) of $S_1 \rightarrow T_n$ ISC has been reported in several luminescent transition metal complexes [28–32], for which, similar to complex **1**, appreciable MLCT% contributes to both S_1 and T_1 states, greatly enhancing the mixing between two spin manifolds.

2.2. $T_1 \rightarrow S_0$ radiative transition

Once populated at the lowest lying triplet state (T_1), one would expect to harvest the $T_1 \rightarrow S_0$ phosphorescence via its radiative transition, the rate constant k_r^p of which can be expressed as [33]:

$$k_r^p \propto < \psi_{S_0} | H_{er} | \psi_{T_1} >^2 \approx \gamma \frac{< \psi_{S_1} \left| H_{so} \right| \psi_{T_1} >^2 \mu_{S_1}^2}{(\Delta E_{S_1-T_1})^2},$$

$$\gamma = \frac{16\pi^3 10^6 n^3 E_{em}^3}{3h\varepsilon_0} \quad (2)$$

where H_{er} denotes the electric dipole operator created by the electric magnetic field. μ_{S_1} is the $S_0 \rightarrow S_1$ transition dipole moment, E_{em} represents the T_1–S_0 energy gap in cm^{-1}, and n, h, and ε_0 are the refractive index, Planck's constant, and the permittivity in vacuum, respectively. More specifically, upon considering the associated vibrational motions in each electronic state, $\mu_{S_1}^2$ can thus be expanded to:

$$\mu_{S_1}^2 \propto | < S_1 \Phi_{S_1 0} | H_{er} | S_0 \Phi_{S_0 m} > |^2 = | < S_1 | H_{er} | S_0 > |^2 FC_{S_1 0, S_0 m} \quad (3)$$

where $FC_{S_1 0, S_0 m}$ specifies the Franck–Condon overlap factor between the vibrational wave function (Φ) of S_1 at the vibrational quanta of $v = 0$ and that of S_0 at $v = m$. Note that S_0 and S_1 in Eq. (3) only denote the electronic wave function. In addition, to simplify the discussion, instead of summation of the entire vibrational states in S_0, only one vibronic state, i.e. m, in S_0 is considered for the transition.

As formulated in Eqs. (2) and (3), k_r^p is then related to the mixing, i.e. the spin–orbit coupling, between S_1 and T_1, the result of which is reminiscent of the theoretical expression regarding $S_1 \rightarrow T_1$ ISC expressed in Eq. (1). This similarity is not surprising. Due to the spin difference in nature between singlet and triplet manifolds, the $T_1 \rightarrow S_0$ radiative transition is virtually null. A partially allowed transition requires breakdown of the spin forbidden rule by borrowing the singlet spin character via mixing T_1 with the proximate state e.g. S_1, a mechanism similar to that of the coupling matrix in dealing with the $S_1 \rightarrow T_1$ ISC. The mixed S_1 character also leads to the dependence of k_r^p on the $S_1 \rightarrow S_0$ transition, i.e. $\mu_{S_1}^2$. As a result, in addition to the spin–orbit coupling matrix, k_r^p is also governed by $S_0 \rightarrow S_1$ transition moment, the energy gap between S_1 and T_1, $(\Delta E_{S_1-T_1})^2$, and the emission energy gap, E_{em}^3.

To emphasize the above relationship, we then exploit a case in point recently encountered in our advances. Among a series of Ir(III) complexes (**7**–**10**, Fig. 2) bearing double benzyldiphenylphosphine cyclometalates (the P^C chelate), intriguing differences in photophysical properties are observed. For example, in comparison to **7** and **8**, the phosphorescence radiative decay rate constants decrease by more than one order of magnitude in **9** and **10**, despite their relatively similar MLCT% calculated for both S_1 and T_1 states (Table 1) [34]. For rationalization, we first assess the spin–orbit coupling matrix term $< \psi_{S_1} | H_{so} | \psi_{T_1} >^2$, defined as SOC, by deducing the corresponding parameters via TDDFT calculation. The results, though having a qualitative manner, reveal a trend of SOC value of **7** (73.63×10^{-4} eV^2) and **8** (247.99×10^{-4} eV^2) > **9** (8.42×10^{-4} eV^2) and **10** (14.62×10^{-4} eV^2). While the calculated MLCT% remains nearly similar, this distinctive difference mainly lies in the different $\pi\pi^*$ character, namely the intra-ligand charge transfer (ILCT) for **9** and **10** versus ligand-to-ligand charge transfer (LLCT) from the benzyl group of P^C chelate to the pyridyl moiety of the N^N chelate in **7** and **8**. Empirically, this trend can be rationalized by the elongation of π-conjugation for isoquinolinyl (**9**) and phenanthridinyl (**10**) derivatives (c.f. pyridyl moiety in **7** and **8**) such that the lowest-lying $\pi \rightarrow \pi^*$ transition is associated with ILCT per se. Evidence from the spectroscopy angle is given by much red-shifted phosphorescence for **9** (599 nm) and **10** (606 nm) relative to **7** (471 nm) and **8** (472 nm).

To gain in-depth insight, the major S_1–T_1 mixing term $<^1 d_\pi \pi^* | H_{so} |^3 \pi\pi^*>$ (or $<^3 d_\pi \pi^* | H_{so} |^1 \pi\pi^*>$) (see Section 2.1) can be further classified into $<^1 d_\pi \pi^* | H_{so} |^3$LLCT> (or $<^3 d_\pi \pi^* | H_{so} |^1$LLCT*>) and $<^1 d_\pi \pi^* | H_{so} |^3$ILCT*> (or $<^3 d_\pi \pi^* | H_{so} |^1$ILCT*>). For the former, as in the cases of **7** and **8**, the ligand-to-ligand transfer may accompany, in part, changes of orbital angular moment, which then couples with the flip of electron spin, leading to the enhancement of S_1–T_1 mixing. Further support of this viewpoint is given by the smaller $\Delta E_{S_1-T_1}$ for **7** (0.18 eV) and **8** (0.38 eV) than those of **9** (0.52 eV) and **10** (0.41 eV). Increase of S_1–T_1 mixing should be proportional to the reduction of the energy gap, i.e. $\Delta E_{S_1-T_1}$, between S_1 and T_1. In brief, the large SOC value, small $\Delta E_{S_1-T_1}$, and hence the increase of $(1/\Delta E_{S_1-T_1})^2$, and increase of E_{em}^3 all are in favor of **7** and **8** to render a larger k_r^p value than that of **9** and **10**, justifying the fundamental concept derived from Eq. (2).

2.3. $T_1 \rightarrow S_0$ nonradiative transition

Using a first-order approximation, the $T_1 \rightarrow S_0$ nonradiative decay constant k_{nr}^p can be expressed as:

$$k_{nr}^p \propto \frac{4\pi^2 \rho_E}{h^2} | < T_1 \Phi_{T_1 0} | H_{nr} | S_0 \Phi_{S_0}(E) > |^2$$

$$= \frac{4\pi^2 \rho_E}{h^2} | < T_1 | H_{nr} | S_0 > |^2 | < \Phi_{T_1 0} | \Phi_{S_0}(E) > |^2$$

$$= \frac{4\pi^2 \rho_E}{h^2} | < T_1 | H_{nr} | S_0 > |^2 FC_{T_1 0, S_0(E)} \quad (4)$$

where H_{nr} is any perturbation Hamiltonian that can induce the jump between two PESs [35–38], and S_0 and T_1 in Eq. (4) only denote the electronic wavefunction. E in $\Phi_{S_0}(E)$ specifies the vibrational energy between the zero point energies of T_1 and S_0. For nonlinear, polyatomic molecules such as the late transition metal complexes covered in this review, due to the 3n-6 degrees of freedom in vibrational motion, there should be a large number of $\Phi_{S_0}(E)$ states being isoenergetic with respect to $\Phi_{T_1 0}$, which may be further broadened by solvent perturbation, converging into a continuum of state density ρ_E. $FC_{T_1 0, S_0(E)}$ is the Franck–Condon overlap factor, which describes the overlap of the continuum of vibrational states $\Phi_{S_0}(E)$ with respect to $\Phi_{T_1 0}$.

Readers can virtually view the Franck–Condon factor as a vertical transition in k_r^p, while it is a horizontal transition in k_{nr}^p. The electronic coupling factors $| < S_0 | H_{er} | T_1 > |^2$ and $| < S_0 | H_{nr} | T_1 > |^2$ for k_r^p and k_{nr}, respectively, involve the wavefunctions of initial (T_1) and final (S_0) electronic states, such that the radiationless transition is subject to the same multiplicity selection rules as the radiative transition [39]. In other words, the stronger S_1–T_1 mixing due to the greater ^{3}MLCT contribution [40,41], in parallel, leads to more singlet character in T_1, resulting in an increase of both k_r and k_{nr}.

The above viewpoint defies a general concept conveyed among many synthetic chemists in that the large k_r^p value usually comes up with greater emission intensity. In reality, increase of k_r^p may also receive a trade-off of increments of k_{nr}^p, such that the phosphorescence Q.Y. ($= k_r^p/(k_r^p + k_{nr}^p)$) is more subtle than intuitively understood by conventional wisdom [42]. We will exemplify this point in the following sections.

2.4. Crucial factors governing nonradiative transition

2.4.1. Role of ^{3}MC dd state

Suppressing any $T_1 \rightarrow S_0$ radiationless deactivation pathways should accordingly increase the designated $T_1 \rightarrow S_0$ phosphorescence yield. This seemingly straightforward approach unfortunately is a non-trivial task. As for the late transition metal complexes, one key factor that commonly promotes radiationless deactivation should be ascribed to the population of the ^{3}MC *dd* excited state [43,44]. Due to its $d_\pi \rightarrow d_{\sigma^*}$ transition in nature, i.e. the anti-bonding character in d_{σ^*} that results in weakening of the metal–ligand interaction, the ^{3}MC *dd* state possesses a repulsive PES. Accordingly, as depicted in Fig. 3, thermal population to the MC *dd* state may thus cause weakening of metal–ligand bonding, and the elongation of the bond distance along the repulsive PES eventually touches PES of the ground state (S_0), inducing the radiationless deactivation.

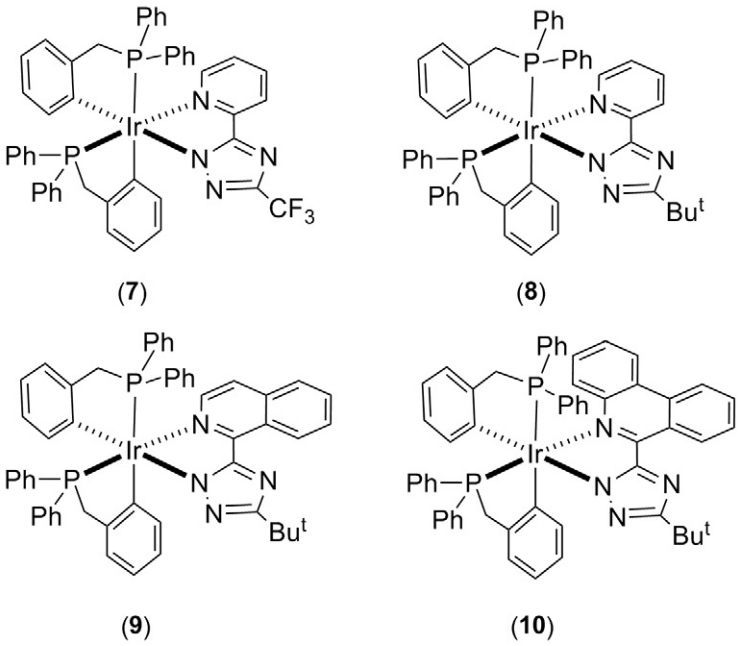

Fig. 2. Structural drawings of Ir(III) metal complexes **7**–**10** bearing double benzyldiphenylphosphine cyclometalates.

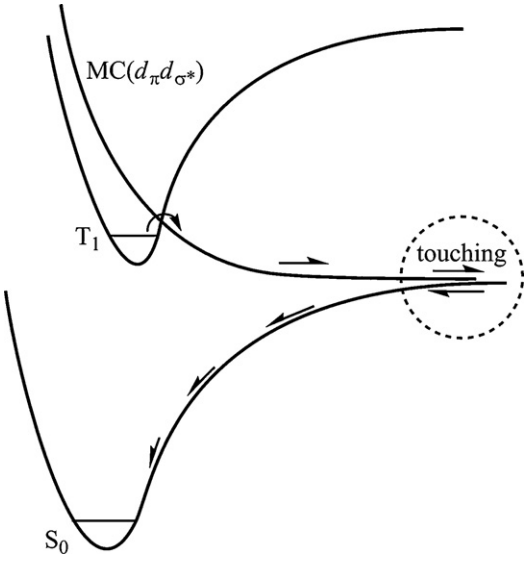

Fig. 3. The population of the repulsive *dd* state from the lower lying states (using T_1 as an example) and the subsequently non-radiative deactivation via touching the potential energy surface of the S_0 state.

There has been significant progress regarding strategic design of the transition metal complexes to avoid the stabilization (lowering) of the ^{3}MC *dd* excited state. This issue is particularly emergent for the Ru(II) based luminescence complexes [45,46] mainly due to their weak ligand field, and hence lowering of the ^{3}MC *dd* state naturally occurs. Relevant advances include: (i) using strong σ-donor ligand to destabilize the ^{3}MC *dd* state, (ii) making the whole complex nearly octahedral, such that the intrinsic crystal field splitting energy ($t_{2g} - e_g$) is enlarged via the generation of near ideal 90° bite angle, and (iii) incorporation of ligands with an extended π-conjugation to reduce ππ* energy, resulting in far separation between the ^{3}MC *dd* state and the corresponding ^{3}MLCT/ππ* emissive states, etc. [47,48].

For the sake of convenience and clarity, we then continuously apply complexes **7**–**10** (see Fig. 2) as prototypes to illustrate the above viewpoints. As shown in Table 1, even though the phosphorescence radiative decay rate constants for **7** and **8** are greater than those of **9** and **10** by a factor of >10, the phosphorescence quantum yields (Q.Y.) are much lower in **7** (0.0014) and **8** (0.011) (c.f. **9**: 0.65 and **10**: 0.41). This discrepancy apparently is due to large nonradiative decay rate constants (k_{nr}) of 8.3×10^8 s^{-1} and 1.3×10^8 s^{-1} for **7** and **8**, respectively, which are greater than k_{nr} (~10^4 s^{-1}) of **9** and **10** by ~4 orders of magnitude. As for the dominant radiationless deactivation in **7** and **8**, we reasonably suspect the proximity between ^{3}MC *dd* state and the designated ^{3}MLCT or ^{3}ππ* emissive states, in which the ^{3}MC *dd* state serves as a major deactivation channel due

Table 1
The experimentally resolved phosphorescence maxima in wavelength, radiative and non-radiative decay rate constants in degassed CH_2Cl_2, together with orbital transition analyses and spin–orbit coupling matrix element of complexes **7**–**10** [34].

	λ_{max}^{em} [a] [nm]	k_r [b] [s^{-1}]	k_{nr} [c] [s^{-1}]	Φ_p [d]	MLCT% (S_1) (T_1)	$< \psi_{S_1} \lvert H_{so} \rvert \psi_{T_1} >^2$ [10^{-4} eV^2]
7	471	1.2×10^6	8.3×10^8	0.0014	(31.32) (15.96)	73.63
8	472	1.4×10^6	1.3×10^8	0.011	(33.61) (18.32)	247.99
9	556, 599	2.9×10^4	1.6×10^4	0.65	(30.50) (12.19)	8.42
10	503	9.3×10^4	1.4×10^5	0.41	(30.74) (14.77)	14.62

The last column represents the spin–orbit coupling matrix.
[a] Emission peak wavelength.
[b] k_r (radiative decay rate constant) = Φ_p/τ_{obs} where τ_{obs} denotes the observed lifetime.
[c] k_{nr} (non-radiative decay rate constant) = $1/\tau_{obs} - k_r$.
[d] Phosphorescence quantum yield.

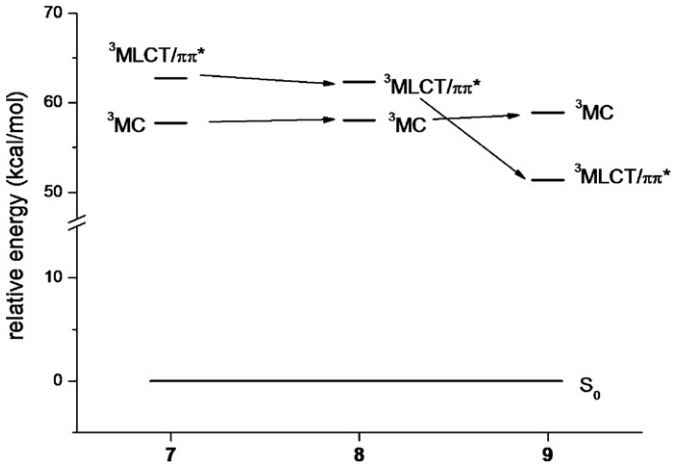

Fig. 4. Energy level for ^{3}MLCT/ππ* versus ^{3}MC *dd* states in Ir(III) complexes **7**–**9**; see the text for a detailed description.

to its repulsive PES. Conversely, for **9** and **10**, the great extension of the π-conjugation by isoquinolinyl (**9**) and phenanthridinyl (**10**) derivatization should decrease the ππ* energy gap and likewise the $d_\pi \rightarrow \pi^*$ MLCT transition, while the energetics of the ^{3}MC *dd* state remain relatively unchanged. Consequently, the ^{3}MC *dd* state is no longer thermally accessible, significantly reducing the nonradiative decay pathways, which in turn leads to a leaping increase of the phosphorescence Q.Y. for **9** and **10**.

The proof of the above concept, i.e. relative energy gap between ^{3}MLCT/ππ* and ^{3}MC *dd* states versus deactivation pathways, can be accessed by recent theoretical advances. In this approach, the electronic configurations of ^{3}MC *dd* states are calculated following Persson's work [49]. In brief, the ^{3}MLCT state geometry is obtained by performing geometry optimization along the triplet state potential energy surface (PES), using the core arrangement derived from the X-ray structural data of **7**, **8** and **9** as the initial geometry. Complex **10** is relatively too complicated to be suited for the following approach. As for the ^{3}MC state, because the electron densities are mainly distributed on the central metal atom, we thus deliberately perform geometry optimization of the ^{3}MC states following the methodology illustrated [50–53]. This calculation starts with a distorted geometry, for which the metal–ligand bonds are largely elongated, such that its associated energy is expected to be far away from the global minimum along the PES. Accordingly, the optimization is able to fall into the presumably shallow local minimum associated with the ^{3}MC *dd* state. The resulting ^{3}MC *dd* structure was further confirmed by the net spin values located on the transition metal according to the Mulliken population analysis.

The results shown in Fig. 4 clearly demonstrate that the energy level of the lower lying, mixed ^{3}MLCT/ππ* state is sensitive to the extension of the π conjugation and tends to decrease from **7**, **8** to **9**, while ^{3}MC *dd* is nearly insensitive to the perturbation of π-extension. As a result, for **7** and **8**, the ^{3}MC *dd* state is below the ^{3}MLCT/ππ* state in energy and may thus be thermally accessible to induce dominant radiationless transition. Conversely, the order of energetics between the ^{3}MLCT/ππ* and ^{3}MC *dd* states is reversed in **9**, in which ^{3}MC *dd* is well above the luminescent ^{3}MLCT/ππ* state and thus makes negligible contribution to the deactivation process, justifying the experimental observation. We have fully exploited the above strategies in designing transition metal complexes, especially those of Ir(III) blue emitting complexes requiring high T_1–S_0 energy gap, and have successfully improved the luminescence properties to attain a true blue OLED [50–53].

Table 2
Photophysical properties of blue-emitting Os(II) complexes **11**–**14** in degassed acetonitrile at RT [55].

	λ_{max}^{abs} [a] [nm]	λ_{max}^{em} [b] [nm]	Q.Y. Φ[c]	τ_{obs} [d] (μs)
13	333	455, 480, 507	0.42	39.9
14	340	460, 483, 515	4.6×10^{-4}	0.026

[a] Absorption peak wavelength.
[b] Emission peak wavelength.
[c] Emission quantum yield.
[d] The observed lifetime.

2.4.2. Bond weakness inducing nonradiative deactivation

Applying similar concept delivered from the ^{3}MC *dd* state, it is then conceivable to null the radiationless deactivation process induced by weakening a specific bond in the lower lying excited states. Herein, the specific bonding effect is exemplified by a series of blue emitting Os(II) complexes, for which the photophysical properties can be drastically varied by implementing the *trans* effect elaborated as follows.

One of our important advances should be credited to the successful reaction between pyridyl azolates chelates and $Os_3(CO)_{12}$, leading to the isolation of blue luminescent Os(II) complexes **11**–**14** (Fig. 5) [54]. As mentioned in Section 2.4.1, highly emissive phosphorescence in blue is achievable if the ^{3}MC *dd* state can be lifted above the lowest lying luminescence state. One of the strategies is to decrease the d_π energy and hence increase the ^{3}MC *dd* level via rational introduction of ancillary ligands. For complexes **11**–**14**, this goal is attained by using CO as the ancillary ligand. CO possesses great π-accepting character and is capable to reduce the electron density in the Os(II) metal centre, further lowering the d_π energy.

Among **11**–**14**, particular attention is paid to probe effects of relative ligand orientation versus photophysical properties. Despite their structural isomerism, remarkable differences in luminescence behavior were resolved between **13** and **14** [55]. As listed in Table 2, complex **13** exhibits strong emission, with a quantum yield of 0.42, for which distinct vibronic peak maxima appeared at ~455, 480, and 507 nm, in degassed CH_3CN at 298 K. With a similar emission frequency and spectroscopic feature, in stark contrast, the emission intensity of **14** is much weaker, showing Q.Y. as low as 4.6×10^{-4} under identical experimental conditions. This weak phosphorescence also correlates well with the observed fast relaxation dynamics, in which the lifetime of phosphorescence for **14** was measured to be as short as 26 ns, as opposed to ~40 μs for **13** in degassed CH_3CN at RT.

One would promptly propose a mechanism in which thermal population to the ^{3}MC *dd* state may play a key role to promote the radiationless transition in **14**. This possibility is ruled out because none of the four lowest excited states, including two singlet and two triplet manifolds based on the DFT calculation, possess the anticipated MC *dd* character. The thermal inaccessibility of the *dd* excited state is believed to be a combination of strong ligand field strength of the azolates and the CO π-accepting property. On the other hand, possibility of phosphorescence quenching by large amplitude motion is also discarded due to the similarly <1/100 emission intensity of **14** (c.f. **13**) in strictly rigid single crystal. As for a plausible rationalization, the lowest energy T_1 state in **14** could be reasonably attributed to a ^{3}ππ* manifold, mixed with a small amount of the ^{3}MLCT character. Thus, population of the T_1 excited state causes the shift of the electron density from the Os(II) metal, CO ligands, and triazolate to the pyridyl moiety acting as a LUMO, resulting in a reduction of both the Os(II)–CO π-bonding and the already weakened pyridine-to-Os(II) metal interactions in **14** due to the *trans*-effect exerted by CO (c.f. **13**). As a result, the potential energy surface of T_1 might be so shallow that a surface crossing between S_0 and T_1 becomes feasible. For clarity, an overall excited-state relaxation process for **14** is depicted in Fig. 6. Upon

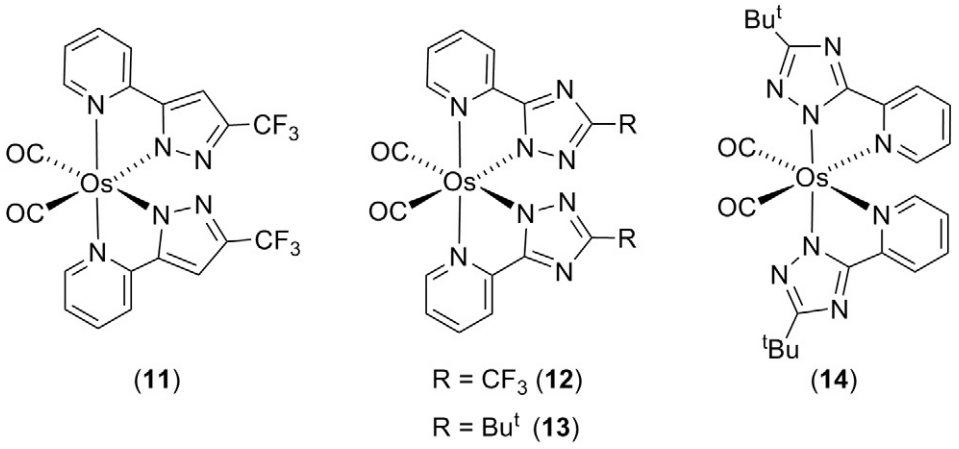

Fig. 5. Structural drawings of Os(II) metal complexes **11**–**14** bearing two pyridyl-azolate chelates.

excitation, fast $S_1 \rightarrow T_n$ intersystem crossing takes place due to the Os enhanced spin–orbit coupling. The computational result [55] also points out that intersystem crossing proceeds from S_1 to T_2 due to their closeness in energy, followed by a fast rate of T_2 to T_1 internal conversion coupled with solvent (phonon vibration in solid) deactivation ($\leq$1 ps^{-1}). Temperature dependent study clearly indicates that $T_1 \rightarrow S_0$ surface crossing via weakening Os(II)–pyridine and/or Os(II)–CO bond, i.e. the "loose bolt" effect [56], is thermally activated with a barrier of 7.6 kcal/mol. At 150 K, the phosphorescence Q.Y. is as high as 0.4 in 3-methyltetrahydrofuran.

Such a quenching process, i.e. the deactivation via bond weakness caused by *trans* effect together with corresponding shift of electron density in the lower lying states, may be commonly encountered for the geometry isomers among late transition metal complexes. For instance, the above observation and delineation allow a parallel comparison with the related complexes [Ir(ppy)$_3$] and [Ir(ppz)$_3$], (ppz)H = N-phenyl pyrazole, for which isolation of two geometrical isomers were also documented [57]. Structural and spectroscopic data suggest that the facial isomers have the stronger and more evenly distributed metal–ligand bonding, exhibiting bright phosphorescence in both fluid and solid states. In contrast, the meridional isomers have much greater bond length alternations caused by the differing *trans* influences of anionic phenyl and neutral N donors (or azolate versus pyridine) and

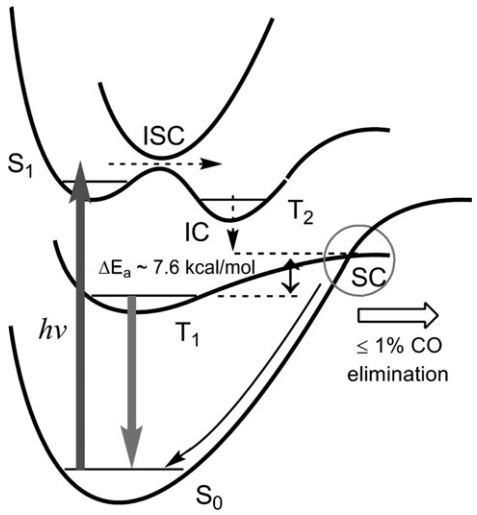

Fig. 6. Energy levels of the lower lying excited states and the proposed relaxation pathway for complex **14**. ISC: intersystem crossing; IC: internal conversion; SC: surface crossing.

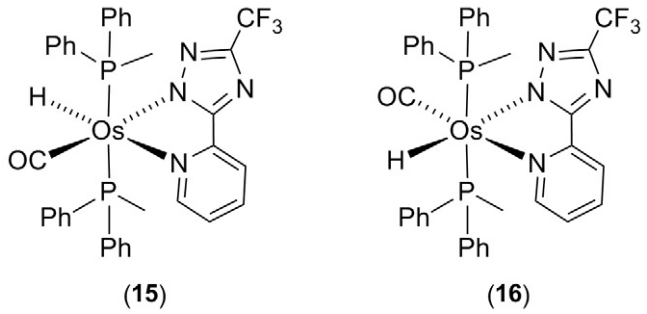

Fig. 7. Structural isomerism of Os(II) metal complexes containing hydride ancillary ligand.

are thus significantly less emissive. Naturally, this greater bond strength alternation of the meridional isomers then exerts a similar "loose bolt" effect to account for their dominant rate of radiationless deactivation.

Additional illustration is given by the Os(II) hydride complexes **15** and **16** (Fig. 7) [58], and their pertinent photophysical properties are listed in Table 3. As for the UV/vis spectra, the absorption peak of 373 nm in **15** is notably red shifted to ~406 nm in **16** (Table 3). For rationalization, the π-accepting CO ligand in **15** leads to a decrease of its *trans*-triazolate π-energy level, while the strong σ-donating hydride ligand would increase its π* energy of the *trans*-pyridyl group, resulting in an increase of the ILCT energy gap. Conversely, an opposite effect is exerted in **16,** for which the π electron deficiency in the pyridyl moiety leads to a decrease of the ILCT gap, consistent with the corresponding absorption spectroscopic differences between **15** and **16**. Likewise, distinctly different emission properties are resolved, in which the emission Q.Y. of **16** (Φ_p ~0.38) is higher than that of **15** (Φ_p ~0.01) by ~40-fold (see Table 3).

To account for the emission properties, time dependent-DFT calculation has shown that the T_1 state in **15** mainly consists of an appreciable portion of CO-to-pyridine LLCT transition, which would reduce the π-accepting strength of the CO ligand and, hence, the

Table 3
Photophysical properties of Os(II) hydride complexes in cyclohexane and solid states at RT [58].

	λ_{max}^{abs} [a] [nm]	λ_{max}^{em} [nm]	Q.Y. Φ	τ_{obs} (μs)
15	273, 307, 373	543 (475)[b]	0.01	0.4
16	265, 303, 406	533 (510)[b]	0.38	6.7

[a] Definition of each column is the same as that in Table 2.
[b] Data in parentheses were measured in solid thin film at room temperature.

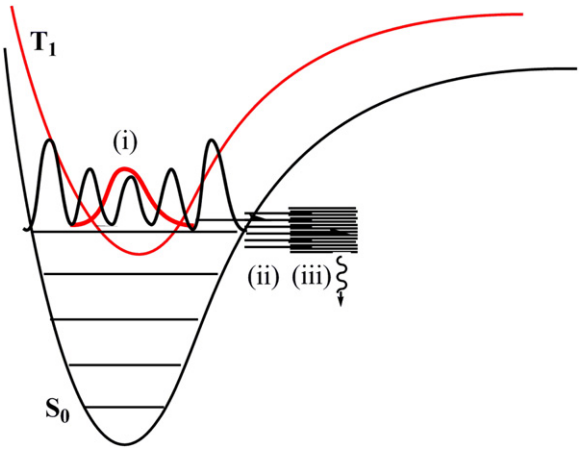

Fig. 8. A general description of energy gap law, using two states T_1 and S_0. The mechanism involves (i) T_1–S_0 vibrational overlap, (ii) coupling with low-frequency, high density vibrations (S_0), and (iii) coupling with solvent collision (or phonon vibration in solid).

weakening Os(II)–CO bond strength would result in a significant distortion of the potential energy surface. In sharp contrast, the T_1 state of **16** involves essentially no contribution from the CO ligand. The results again manifest the specific weak metal–ligand bond that triggers a similar loose bolt effect [56], resulting in an increase of the radiationless transition. Special attention needs to be brought here to the fact that such a bond-weakening effect is rather specific and selective, which stringently depends on the molecular structure and its associated excited-state behavior, and the existence of the ^{3}MC *dd* state is intrinsic in the transition metal complexes.

2.4.3. Quenching via vibrational matching: the energy gap law

In addition to the abovementioned quenching mechanisms, T_1 is subject to radiationless deactivation triggered by the vibrational matching (overlap) between T_1 and the ground state. This process is intrinsic and is operative effectively so long as the two PES involved in the transition (T_1 and S_0 heretofore in this review) have no intersection, i.e. a matching type between two PES, which is normally true for T_1 and S_0 due to their well separated energy. As a result, the main perturbation operator (H_{nr}) contributed to the coupling matrix $|<T_1|H_{nr}|S_0>|^2$ (see Eq. (4)) is the nuclear kinetic energy operator. $|<T_1|H_{nr}|S_0>|^2$ is thus considered to be rather small and accordingly, the Franck–Condon overlap term $FC_{T_1 0,S_0(E)}$ becomes crucial in navigating the deactivation process. The Franck–Condon overlap term, $FC_{T_1 0,S_0(E)}$, increases as the T_1–S_0 energy gap decreases. This is especially effective for high frequency vibrational stretching modes, such as C–H, O–H and N–H, etc. due to the fact that only fewer vibrational quanta (in S_0) are required to reach the zero-point energy of T_1, enhancing the overlapping probability. For example, the C–H bond commonly exists in ligands. Taking its frequency of 3000 cm^{-1} in general and assuming harmonic PES at least for the lower lying vibrational states, its third overtone ($\nu = 4$) has reached 12,000 cm^{-1} (~833 nm), inducing a favorable overlap of vibronic wavefunctions in far visible and near infrared regions (see Fig. 8). As a result, if the nonradiative pathway is only governed by vibrational matching, k_{nr} is expected to be increased as the emission energy gap decreases, which is conventionally dubbed as the energy gap law [35,59–61]. Conversely, as the emission gap decreases, the radiative decay rate constant k_r decreases due to the decrease of the E^3_{em} value (see γ term in Eq. (2)), which is naturally occurring in spontaneous emission. Combining these two factors, the emission quantum yield, defined as Q.Y. $= k_r/(k_r + k_{nr})$, is accordingly decreased upon decreasing the emission energy gap.

For polyaromatic organic molecules, the rate of $S_1 \rightarrow S_0$ internal conversion governed by energy gap law can be empirically expressed as $k_{nr} \sim 10^{13} e^{-\alpha \Delta E}$ where α is the proportionality constant and is taken to be ~0.18, and ΔE is the S_1–S_0 energy gap in terms of kcal/mol [56]. At the current stage, an empirical approach to estimate the energy gap regarding forbidden T_1–S_0 deactivation is still pending. In a qualitative manner, however, using a similar expression for the $S_1 \rightarrow S_0$ internal conversion, we may be able to assess its rate constant (k^p_{nr}) by taking:

$$k^p_{nr} \sim F_{spin} 10^{13} e^{-\alpha \Delta E} \quad (5)$$

where ΔE is the T_1–S_0 energy gap in terms of kcal/mol, and F_{spin} denotes a spin forbidden factor, the latter is defined as $F_{spin} = k^p_r/k^f_r$ where k^p_r and k^f_r denote radiative decay rate constants of phosphorescence and fluorescence, respectively. Taking the onset of phosphorescence to be 600 nm ($\Delta E \sim 47.6$ kcal/mol), for example, the second term in Eq. (5), i.e. $10^{13} e^{-\alpha \Delta E}$, is then calculated to be $\sim 1.9 \times 10^9\ s^{-1}$. For a pure qualitative approach, we simply assume k^p_r and k^f_r to be $10^5\ s^{-1}$ and $10^8\ s^{-1}$, which is a reasonable value if one considers the conventional radiative lifetime of phosphorescence and fluorescence, respectively, for late transition metal complexes. This gives $F_{spin} = k^p_r/k^f_r = \sim 10^{-3}$. Accordingly, k^p_{nr} (Eq. (5)) is deduced to be $1.9 \times 10^6\ s^{-1}$ and Q.Y. of the phosphorescence ($= k^p_r/(k^p_r + k^p_{nr})$) is thus calculated to be ~0.05. Evidently, the energy gap law has influenced the emission yield appreciably. In theory, Q.Y. should drop exponentially upon further lowering the energy gap, manifesting the importance and effectiveness of energy gap law operated in the deep-red and near infrared region.

3. Relaxation in high lying states

Heretofore, focus is mainly on the relaxation pathways of the lowest lying excited state in both singlet and triplet manifolds. Due to the complexity of transition metal complexes, in which the metal core can be anchored by multiple chromophores, such that energy transfer, electron transfer and intersystem crossing may thus take place via inter-ligand, intra-ligand and even ligand-to-metal pathways, gaining fundamental insight into the dynamics of relaxation in the high-lying electronic states is becoming of pivotal importance. Special attention is paid to the luminescent transition metal complexes coordinated by multiple latent emitting chromophores. Whether one should treat the whole complex as a single entity or a metal core attached by a distinctive unit of each chromophore has recently received much attention. The latter issue is of particular interest if one's goal is to attain the multiple emission color. In this case, due to the possible lack of state mixing, dynamics of energy/electron transfer may be rather slow, and each individual chromophore may have its own contribution to achieve the panchromatic emission.

Recently, exploiting a series of Ir(III) based complexes, tuning of emission colors over the entire visible spectra has been achieved by modification of both heteroaromatic cyclometalates and the third chelating anions that are generally represented by C^N and L^X, respectively [62–67]. Among these efforts, a rather slow, i.e. at the time scale of nanoseconds, interligand energy transfer (ILEnT) mechanism (see Fig. 9A) has been proposed to illustrate the color tuning from 468 to 666 nm in the system of $[Ir(dfppy)_2(L^X)]$, where dfppy = 2-(2,4-difluorophenyl)pyridinato and L^X = picolininate, quinaldinate, isoquinolinate, or pyrazinate chelate [68,69]. Implicitly, this proposed mechanism is prone to a system in which a central Ir(III) metal core is coordinated by distinctive chromophores with rather weak inter-chelate interaction. The concept behind would raise a brightening possibility for latent application in multiple luminescence.

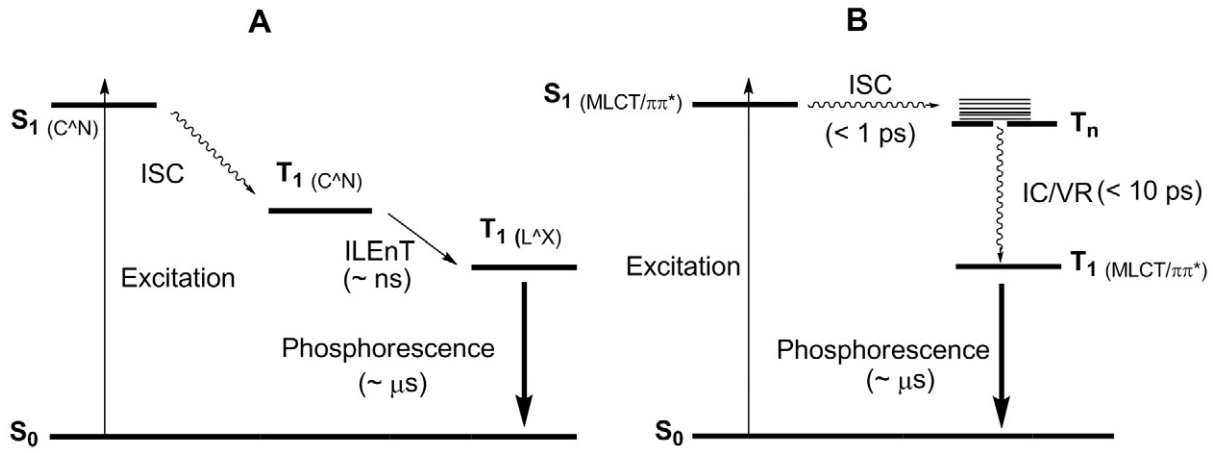

Fig. 9. (A) The proposed slow energy transfer mechanism incorporating C^N and L^X types of ligands. (B) A revised scheme based on conventional relaxation mechanism [68]. Reprint permission issued by the American Chemical Society.

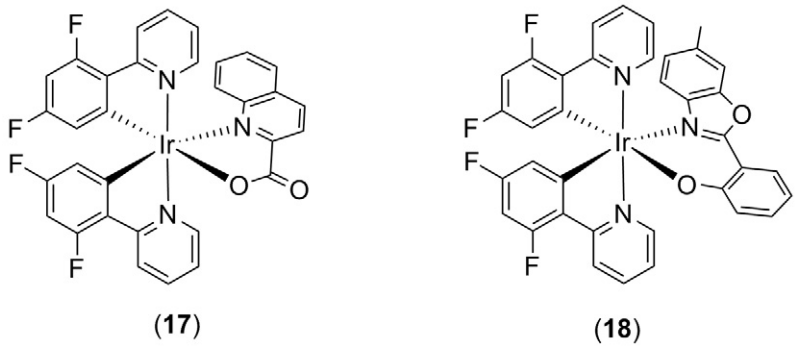

Fig. 10. Structural drawings of Ir(III) complexes **17** and **18** [68]. Reprint permission issued by the American Chemical Society.

However, upon further detailed investigation into the relaxation dynamics of two prototypical complexes (Fig. 10) with L^X = quinaldinate (**17**) and 2-(6-methylbenzoxazol-2-yl)phenolate (**18**), and using transient absorption and time-resolved emission spectroscopy covering the entire time range from picoseconds to microseconds, population of the lowest triplet state is achieved via ultrafast $S_1 \rightarrow T_n$ intersystem crossing (<1 ps) followed by a rapid $T_n \rightarrow T_1$ internal conversion/vibrational relaxation in less than 10 ps [70]. Frontier orbital analyses also indicate strong mixing among ligand chromophores (ancillary ligands included) and core metal orbitals in the majority of higher lying excited states. Thus, these transition metal complexes should have frontier orbitals effectively communicating through the central metal ion; therefore, the photophysical properties can be adequately described by a conventional relaxation mechanism, such as that of polyatomic molecules in the condensed phase [71], which generally incorporates fast internal conversion (IC) and vibrational relaxation (VR) processes of <10 ps to the lowest lying excited state under the same spin manifold. In other words, the conventional relaxation scheme depicted in Fig. 9B, rather than the proposal of slow ILEnT (Fig. 9A), can sufficiently rationalize the experimental observations [70].

Nevertheless, we acknowledge that energy transfer with a relatively slow time scale does occur for complexes with chromophoric pendant linked by alkyl spacer, since the chromophores retain their individual characteristics. For instance, for Cu(I) complex **19** (Fig. 11) incorporating dimethylene-anthracene derivatized 1,10-phenanthrolines, transient absorption studies by McClenaghan et al. [72] reveal an additional 60 ps time constant following the 15 ps ^{1}MLCT $\rightarrow$ ^{3}MLCT intersystem crossing versus that observed in the parent complex **20**. The 60 ps dynamics lead to the temporal spectroscopic evolution resembling that of the $^3\pi\pi^*$ state of the sole anthracene moiety, verifying the attribution of this process to ^{3}MLCT $\rightarrow$ $^3\pi\pi^*$ energy transfer. Moreover, the steady-state absorption spectrum of **19** is essentially the summation of **20** and free anthracene, further demonstrating that slow energy transfer

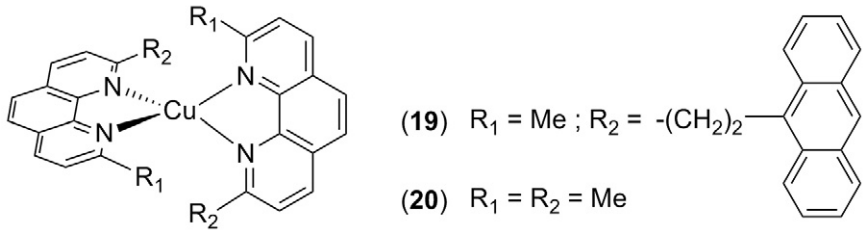

Fig. 11. Structural drawings of Cu (I) complexes **19** and **20** [72]. Reprint permission issued by the American Chemical Society.

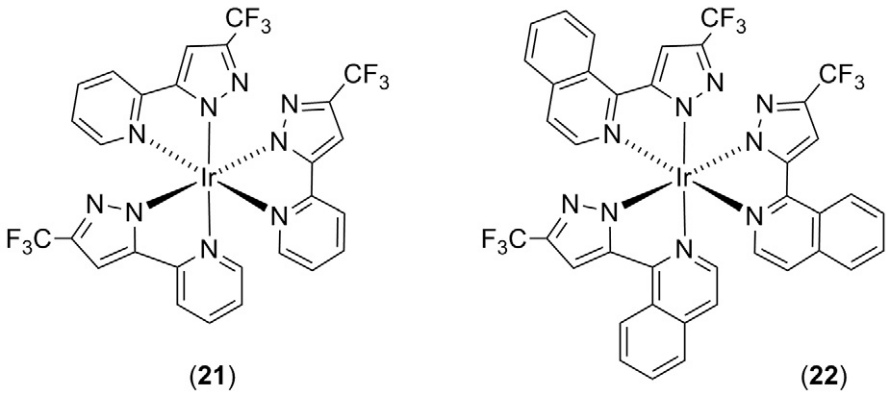

Fig. 12. Structures of Ir(III) complexes **21** and **22** bearing three pyridyl-azolate ligands.

takes place only in cases where chromophores are well-separated by saturated spacers.

The above mentioned energy-transfer time scale of several tens of picoseconds is still much faster than typical radiative lifetime of e.g. microseconds for the phosphorescence observed for the late transition metal complexes. So, practically speaking, generation of dual/multiple phosphorescence emissions in one entity of a complex is not a trivial task at all. In theory, one feasible route of achieving e.g. dual phosphorescence is to ingeniously design transition metal complexes such that two lower lying triplet states are close in energy but possess different types of orbital transition in nature, for example purely ^{3}ILCT and ^{3}LLCT, and in each state with small or even negligible involvement of metal d_π orbital (e.g. ^{3}MLCT) that plays a key intermingling element for state mixing. Such a configuration, in theory, should lead to relatively slow rate of conversion between two states (^{3}ILCT and ^{3}LLCT) due to the lack of electronic coupling. This viewpoint can be exemplified by the recently developed meridional Ir(III) complex **21** (Fig. 12) bearing three pyridyl azolate ligands [73].

The spectroscopic data of **21** and its triazolate analogues demonstrate remarkably dual phosphorescence, i.e. blue (430 nm, P_1) and green (530 nm, P_2) bands deriving from the intra-ligand and ligand-to-ligand charge transfer states, i.e. ^{3}ILCT and ^{3}LLCT, respectively, for which the ^{3}ILCT and ^{3}LLCT states are virtually orthogonal to each other with a small extent of ^{3}MLCT. As estimated by TD-DFT calculation, the P_1 state is preferentially populated after vertical (Franck–Condon) excitation at RT, followed by ^{3}ILCT → ^{3}LLCT conversion with a barrier of ~6.9 kcal/mol, possibly induced by certain large-amplitude motions that break down the molecular symmetry and, thus, facilitate the transition. Dynamically, the rate of ^{3}ILCT → ^{3}LLCT internal conversion is expected to decrease upon lowering the temperature, which then makes the P_1 band the dominant decay process at lower temperature. This scenario involving conversion of two weakly coupled states in the lowest triplet manifold is depicted in Fig. 13. Note that the abscissa in Fig. 13 is arbitrary and is only used to emphasize the distinctly different geometric distortion between ^{3}ILCT and ^{3}LLCT along a specific bond length.

Upon extending the π-conjugation by replacing pyridyl in **21** with isoquinolinyl moiety, forming the relevant isoquinolinyl pyrazolate derivative *mer*-[Ir(fipz)$_3$] (**22**), (fipz)H = 3-trifluoromethyl-5-(1-isoquinolyl) pyrazole [74], in sharp contrast, this derivative exhibits a single orange luminescence with Q.Y. as high as 50% in degassed CH_2Cl_2 solution at RT, for which the emission spectrum shows notable vibronic features from the ligand-centred dominant transition. Though pending resolution, it is likely that greater π-conjugation of the fipz chelate somewhat brings ^{3}ILCT and ^{3}LLCT to degeneracy/resonance, resulting in the mergence of two states. The very high emission Q.Y. for **22** can qualitatively be rationalized by the elongation of π-conjugation in the isoquinolinyl pyrazolate moiety, giving T_1 much lower in energy than the MC *dd* excited state.

4. General guideline and the perspectives

In this final discussion section, we summarize previous sections and present a general guideline to the readership regarding the manipulation of excited-state relaxation pathways. Accordingly, several perspectives are based on this guiding concept.

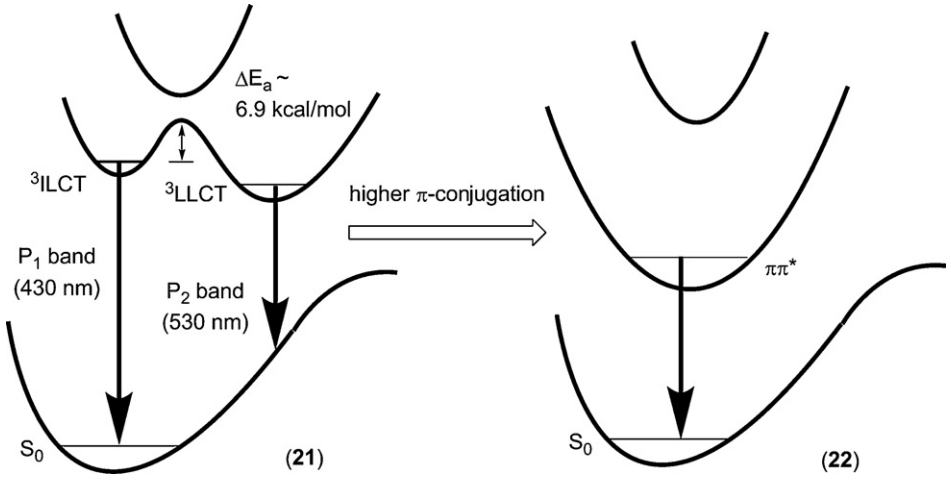

Fig. 13. The proposed relaxation scheme of dual and single phosphorescence for complexes **21** and **22**, respectively.

In the late transition metal complexes, due to the fact that the metal d_π orbital is involved in the majority of electronic transitions, the core metal ion virtually acts as a bridge to network those frontier orbitals associated with all chelating chromophores. For this case, the entire complex can be treated as a single entity, in which the coupling among each vibronic state is sufficiently strong, such that the dynamics of all relaxation processes in the highly excited states, despite the fact that they may associate with different transitions, e.g. MLCT, ILCT and LLCT, etc. are similar to those of π-conjugated polyatomic molecules. This delineation is somewhat different from the photophysics observed in the boron complexes or the *spiro*-bifluorene complexes if one considers boron and carbon atoms, respectively, to be the central core in a way like metal ion in the late transition metal complexes. For example, using the aforementioned pyridyl pyrazolates as ligands, a series of boron complexes have been synthesized, and they exhibit remarkable dual fluorescence properties due to the concomitant photoinduced electron transfer (PET) reaction from pyridyl to the phenyl moiety [75]. The slow time scale (a few hundred picoseconds) of PET indicates that each chromophoric chelate anchoring on the central boron atom can be treated as separated entity. Similar PET phenomena have been reported in *spiro*-bifluorenes anchored by donor and acceptor [76,77]. This may not be surprising since both central boron and carbon atoms possess much higher oxidation potentials and thus make virtually no contribution to the lower lying electronic transitions, giving rather weak coupling among the anchoring chromophores.

In condense phase, upon electronic excitation, the transition metal complex thus undergoes fast intramolecular vibrational redistribution (IVR), internal conversion (IC) and vibrational relaxation (VR) to the lowest lying singlet excited state, i.e. the S_1 state. Subsequently, the $S_1 \rightarrow S_0$ radiative (fluorescence), non-radiative (heat) or $S_1 \rightarrow T_n$ ($n \geq 1$) ISC takes place. All IVR, IC and ISC can be treated as isoenergetic processes, while VR is an energy dissipation process to the surroundings. In solution, VR is operative via coupling with the solvent collision, while it is coupled with the lattice phonon motion to dissipate the energy (heat) in solid. Albeit common in fundamentals with respect to polyatomic organic molecules, subtle differences can be perceived for the titled late transition metal complexes. First of all, due to the much enhancing spin–orbit coupling, the coupling matrices between singlet and triplet manifolds are large. This is especially true for those transitions involving metal d_π orbital, causing the strong mixing between singlet and triplet manifolds. For this case, strictly speaking, pure singlet and triplet states are ill-defined due to the strong state mixing, and the rate of ISC is much faster than ordinary organic molecules. This is known for a number of late transition metal complexes in that the S_1 state possesses a great percentage of MLCT character and the rate of intersystem crossing is measured to be ultrafast (<100 fs, vide supra) [78].

For all cases, the direct involvement of metal d_π orbital plays a key role in harnessing relaxation pathways. Support of this viewpoint is provided by strategic design of Os(II) complexes anchored by strong π-accepting ligands such as carbon monoxide. As a result, the metal d_π orbital is lowered in energy such that the S_1 state possesses mainly the $\pi\pi^*$ character, instead of the aforementioned MLCT character. Accordingly, as described in Section 2.1, the rate of ISC in S_1 for the corresponding Os(II) complexes (see Fig. 1) is reduced drastically to a few to several hundred picoseconds, resulting in dual emission, i.e. both the fluorescence and phosphorescence [26,27].

An intriguing thought thus occurs: what if the contribution of MLCT (or any transition involving d orbital) is negligible in the S_1 state but is great in the highly electronic excited states (S_n, $n > 1$)? One would reasonably expect that time scale of ISC in S_n may need only a few picoseconds or even less, and become a competitive channel with respect to other deactivation processes (IC, VR, etc.) that are commonly dominant in the organic molecules. Thus, upon high energy excitation to S_n, the prompt ISC to the T_m ($m \geq 1$) state may result in the direct population of the lowest lying triplet state. If the efficiency between $S_n \rightarrow T_m \rightarrow T_1$ and $S_n \rightarrow S_1 \rightarrow T_1$ pathways is different, the population ratio for S_1 versus T_1, i.e. the fluorescence versus phosphorescence intensity, should be excitation energy dependent. This consequence may have a great impact in both fundamental, for instance the relaxation dynamics, and latent applications. For the latter, color tuning may be achieved via the ratiometric changes for fluorescence versus phosphorescence as a function of e.g. the applied voltage in OLEDs.

Secondly, due to the repulsive nature, the elongation of ^{3}MC ($d_\pi d_{\sigma^*}$) PES results in contact with the dissociation level of the ground state (S_0), serving as a major radiationless deactivation channel. This is commonly encountered in the late transition metal complexes and especially serves as a major hurdle to attain true-blue emission. The ^{3}MC energy is subject to the bonding between ligand and metal ion, i.e. the ligand field strength. Thus, in addition to altering metal ion, one obvious strategy is to increase the ligand bonding strength. While the available types of ligands may be limited, an alternative and feasible strategy may lie in the exploitation of terdentate or even multi-dentate chelates instead of commonly applied bi-dentate ones. This strategy may also eliminate the latent quenching process via weakness of specific metal–ligand bonding.

Nevertheless, other nonradiative deactivation channels cannot be ignored if one's aim is to strategically design molecules and route to unitary emission Q.Y. Upon tuning the phosphorescence to the near-infrared region, due to the small T_1–S_0 energy gap [35,59–61], one inevitable quenching mechanism is ascribed to the operation of the energy gap law. Several attempts have been made via deuteration and/or fluorination of the emitting complexes; the results unfortunately are not very successful [79–82]. In our viewpoint, one obstacle may lie in the synthetic difficulty, so the deuteration/fluorination was done only partially on specific chromphores. Knowing that the electron density may be delocalized throughout the complex, which is quite possible for the near-IR phosphorescence emitters due to the greatly extended π-conjugation [83,84], full deuteration/fluorination of the entire complex may be necessary to sufficiently suppress the operation of the energy gap law. Such an approach has its fundamental impact but pragmatically is not cost-effective. Moreover, in reality, the operation of the energy gap law per se might be more complicated. In addition to the high frequency vibration modes participating in the quenching process, those of combinational modes with accessible energy may equivalently cause effective quenching, which are less affected by the deuteration/fluorination.

Last but not least, one should not ignore the quenching of emission resulting from the low-frequency vibronic states in S_0, each of which provides very slim coupling with respect to T_1. However, union is strength; the sum of these high density states may surpass other radiationless channels. To suppress this deactivation channel, one conventional strategy is to increase the rigidity of molecular framework [85]. At first glance, this seems to be spontaneously achieved in the solid state, in which large amplitude molecular motions are "frozen" due to the tight packing. Nonetheless, care has to be taken in that certain low frequency vibrations with high density of states, such as partial torisonal or bending motions, require rather small amplitudes and might still be active in the solid state [53]. In addition, specific lattice packing (such as dimer and excimer, etc.) as well as defects on the surface may also serve as additional quenching channels [86]. The former may be suppressed via the introduction of rigid and bulky substituents to the complex. Since this topic is beyond the scope of this review, further in-depth discussion is not elaborated here.

5. Conclusion

We feel responsible for fully acquainting the readers with the fact that precise evaluation of the excited-state relaxation pathways, and hence, accurate control of the emission Q.Y., is still not realistic at this stage. This is particularly true for the metal complexes, due to their structural complexity and anomalously large spin–orbit coupling. Therefore, any computation approach is still in a primitive stage. Taking an obvious and simple example, the oscillation strength f of e.g. $S_0 \rightarrow T_1$ transition is strictly zero in e.g. TDDFT approach due to the bias treatment of zero spin–orbit coupling, which is apparently contradictory to the non-negligible S_0–T_1 absorption commonly observed in the late transition metal complexes. Instead, we intend to provide general guidelines for assessing the emission efficiency, in a qualitative manner, by predicting possible radiationless deactivation pathways. Thus using the aforementioned theoretical and empirical bases, readers in the relevant fields are capable of making profound improvements in the existing designs and harvesting the excitation energy in terms of light more efficiently. Such a rational approach should attain the goal more quickly than simply shooting in the dark.

Acknowledgements

We are grateful for the financial support from the National Science Council and the Ministry of Economic Affairs.

References

[1] R.C. Evans, P. Douglas, C.J. Winscom, Coord. Chem. Rev. 250 (2006) 2093.
[2] P.-T. Chou, Y. Chi, Eur. J. Inorg. Chem. (2006) 3319.
[3] W.-Y. Wong, Dalton Trans. (2007) 4495.
[4] J.A.G. Williams, S. Develay, D.L. Rochester, L. Murphy, Coord. Chem. Rev. 252 (2008) 2596.
[5] Y. You, S.Y. Park, Dalton Trans. (2009) 1267.
[6] W.-Y. Wong, C.-L. Ho, J. Mater. Chem. 19 (2009) 4457.
[7] E. Baranoff, J.-H. Yum, M. Grätzel, M.K. Nazeeruddin, J. Organomet. Chem. 694 (2009) 2661.
[8] C. Ulbricht, B. Beyer, C. Friebe, A. Winter, U.S. Schubert, Adv. Mater. 21 (2009) 4418.
[9] L. Duan, L. Hou, T.-W. Lee, J. Qiao, D. Zhang, G. Dong, L. Wang, Y. Qiu, J. Mater. Chem. 20 (2010) 6392.
[10] Z.-Q. Chen, Z.-Q. Bian, C.-H. Huang, Adv. Mater. 22 (2010) 1534.
[11] Y. Chi, P.-T. Chou, Chem. Soc. Rev. 39 (2010) 638.
[12] P.-T. Chou, Y. Chi, Chem. Eur. J. 13 (2007) 380.
[13] Y. Chi, P.-T. Chou, Chem. Soc. Rev. 36 (2007) 1421.
[14] W.-Y. Wong, C.-L. Ho, Coord. Chem. Rev. 253 (2009) 1709.
[15] N. Armaroli, G. Accorsi, F. Cardinali, A. Listorti, Top. Curr. Chem. 280 (2007) 69.
[16] A. Vogler, H. Kunkely, Coord. Chem. Rev. 200–202 (2000) 991.
[17] A. Vogler, H. Kunkely, Top. Curr. Chem. 213 (2001) 143.
[18] D.J. Stufkens, A.J. Vlček, Coord. Chem. Rev. 177 (1998) 127.
[19] A.J. Vlček, S. Záliš, Coord. Chem. Rev. 251 (2007) 258.
[20] G. Zhou, W.-Y. Wong, S.-Y. Poon, C. Ye, Z. Lin, Adv. Funct. Mater. 19 (2009) 531.
[21] S.-W. Li, Y.-M. Cheng, Y.-S. Yeh, C.-C. Hsu, P.-T. Chou, S.-M. Peng, G.-H. Lee, Y.-L. Tung, P.-C. Wu, Y. Chi, F.-I. Wu, C.-F. Shu, Chem. Eur. J. 11 (2005) 6347.
[22] S. Reineke, G. Schwartz, K. Walzer, K. Leo, Appl. Phys. Lett. 91 (2007) 123508.
[23] S.P. McGlynn, T. Azumi, M. Kinoshita, Molecular Spectroscopy of the Triplet State, Prentice Hall, Inc., Englewood Cliffs, NJ, 1969, p. 189 (Chapter 5).
[24] T. Yutaka, S. Obara, S. Ogawa, K. Nozaki, N. Ikeda, T. Ohno, Y. Ishii, K. Sakai, M. Haga, Inorg. Chem. 44 (2005) 4737.
[25] H.-L. Yu, Y. Chi, C.-S. Liu, S.-M. Peng, G.-H. Lee, Chem. Vapor Depos. 7 (2001) 245.
[26] Y.-L. Chen, C. Sinha, I.-C. Chen, K.-L. Liu, Y. Chi, J.-K. Yu, P.-T. Chou, T.-H. Lu, Chem. Commun. (2003) 3046.
[27] Y.-L. Chen, S.-W. Li, Y. Chi, Y.-M. Cheng, S.-C. Pu, Y.-S. Yeh, P.-T. Chou, ChemPhysChem 6 (2005) 2012.
[28] N.H. Damrauer, G. Cerullo, A. Yeh, T.R. Boussie, C.V. Shank, J.K. McCusker, Science 275 (1997) 54.
[29] N.H. Damrauer, J.K. McCusker, J. Phys. Chem. A 103 (1999) 8440.
[30] A.T. Yeh, C.V. Shank, J.K. McCusker, Science 289 (2000) 935.
[31] A.C. Bhasikuttan, M. Suzuki, S. Nakashima, T. Okada, J. Am. Chem. Soc. 124 (2002) 8398.
[32] K.-C. Tang, K.-L. Liu, I.-C. Chen, Chem. Phys. Lett. 386 (2004) 437.
[33] S. Haneder, E.D. Como, J. Feldmann, J.M. Lupton, C. Lennartz, P. Erk, E. Fuchs, O. Molt, I. Münster, C. Schildknecht, G. Wagenblast, Adv. Mater. 20 (2008) 3325.
[34] J.-Y. Hung, C.-H. Lin, Y. Chi, M.-W. Chung, Y.-J. Chen, G.-H. Lee, P.-T. Chou, C.-C. Chen, C.-C. Wu, J. Mater. Chem. 20 (2010) 7682.
[35] E.M. Kober, J.V. Caspar, R.S. Lumpkin, T.J. Meyer, J. Phys. Chem. 90 (1986) 3722.
[36] B.R. Henry, W. Siebrand, in: J.B. Birks (Ed.), Organic Molecular Photophysics, vol. 1, Wiley, New York, 1973 (Chapter 4).
[37] K.F. Freed, J. Jortner, J. Chem. Phys. 52 (1970) 6272.
[38] M. Bixon, J. Jortner, J. Chem. Phys. 48 (1968) 715.
[39] J.B. Birks, Photophysics of Aromatic Molecules, Wiley-Interscience, London and Colchester, UK, 1970, p. 151.
[40] T. Azumi, H. Miki, Top. Curr. Chem. 191 (1997) 1.
[41] E.I. Solomon, A.B.P. Lever, Inorganic Electronic Structure and Spectroscopy, vol. 1, John Wiley & Sons, New York, 1999 (Chapter 1).
[42] Y.-M. Cheng, E.Y. Li, G.-H. Lee, P.-T. Chou, S.-Y. Lin, C.-F. Shu, K.-C. Hwang, Y.-L. Chen, Y.-H. Song, Y. Chi, Inorg. Chem. 46 (2007) 10276.
[43] L. Salassa, C. Garino, G. Salassa, R. Gobetto, C. Nervi, J. Am. Chem. Soc. 130 (2008) 9590.
[44] T. Sajoto, P.I. Djurovich, A.B. Tamayo, J. Oxgaard, W.A. Goddard, M.E. Thompson, J. Am. Chem. Soc. 131 (2009) 9813.
[45] E.Y. Li, Y.-M. Cheng, C.-C. Hsu, P.-T. Chou, G.-H. Lee, I.-H. Lin, Y. Chi, C.-S. Liu, Inorg. Chem. 45 (2006) 8041.
[46] K.-C. Hwang, J.-L. Chen, Y. Chi, C.-W. Lin, Y.-M. Cheng, G.-H. Lee, P.-T. Chou, S.-Y. Lin, C.-F. Shu, Inorg. Chem. 47 (2008) 3307.
[47] Y.-L. Tung, S.-W. Lee, Y. Chi, L.-S. Chen, C.-F. Shu, F.-I. Wu, A.J. Carty, P.-T. Chou, S.-M. Peng, G.-H. Lee, Adv. Mater. 17 (2005) 1059.
[48] Y.-L. Tung, L.-S. Chen, Y. Chi, P.-T. Chou, Y.-M. Cheng, E.Y. Li, G.-H. Lee, C.-F. Shu, F.-I. Wu, A.J. Carty, Adv. Funct. Mater. 16 (2006) 1615.
[49] M. Abrahamsson, M.J. Lundqvist, H. Wolpher, O. Johansson, L. Eriksson, J. Bergquist, T. Rasmussen, H.C. Becker, L. Hammarström, P.O. Norrby, B. Åkermark, P. Persson, Inorg. Chem. 47 (2008) 3540.
[50] C.-F. Chang, Y.-M. Cheng, Y. Chi, Y.-C. Chiu, C.-C. Lin, G.-H. Lee, P.-T. Chou, C.-C. Chen, C.-H. Chang, C.-C. Wu, Angew. Chem. Int. Ed. 47 (2008) 4542.
[51] Y.-C. Chiu, Y. Chi, J.-Y. Hung, Y.-M. Cheng, Y.-C. Yu, M.-W. Chung, G.-H. Lee, P.-T. Chou, C.-C. Chen, C.-C. Wu, H.-Y. Hsieh, ACS Appl. Mater. Int. 1 (2009) 433.
[52] Y.-C. Chiu, J.-Y. Hung, Y. Chi, C.-C. Chen, C.-H. Chang, C.-C. Wu, Y.-M. Cheng, Y.-C. Yu, G.-H. Lee, P.-T. Chou, Adv. Mater. 21 (2009) 2221.
[53] Y.-C. Chiu, C.-H. Lin, J.-Y. Hung, Y. Chi, Y.-M. Cheng, K.-W. Wang, M.-W. Chung, G.-H. Lee, P.-T. Chou, Inorg. Chem. 48 (2009) 8164.
[54] P.-C. Wu, J.-K. Yu, Y.-H. Song, Y. Chi, P.-T. Chou, S.-M. Peng, G.-H. Lee, Organometallics 22 (2003) 4938.
[55] J.-K. Yu, Y.-H. Hu, Y.-M. Cheng, P.-T. Chou, S.-M. Peng, G.-H. Lee, A.J. Carty, Y.-L. Tung, S.-W. Lee, Y. Chi, C.-S. Liu, Chem. Eur. J. 10 (2004) 6255.
[56] N.J. Turro, Modern Molecular Photochemistry, University Science Books, 1991 (Chapter 6).
[57] A.B. Tamayo, B.D. Alleyne, P.I. Djurovich, S. Lamansky, I. Tsyba, N.N. Ho, R. Bau, M.E. Thompson, J. Am. Chem. Soc. 125 (2003) 7377.
[58] F.-C. Hsu, Y.-L. Tung, Y. Chi, C.-C. Hsu, Y.-M. Cheng, M.-L. Ho, P.-T. Chou, S.-M. Peng, A.J. Carty, Inorg. Chem. 45 (2006) 10188.
[59] J.V. Caspar, E.M. Kober, B.P. Sullivan, T.J. Meyer, J. Am. Chem. Soc. 104 (1982) 630.
[60] J.V. Caspar, T.J. Meyer, J. Phys. Chem. 87 (1983) 952.
[61] S.R. Johnson, T.D. Westmoreland, J.V. Caspar, K.R. Barqawi, T.J. Meyer, Inorg. Chem. 27 (1988) 3195.
[62] F.-M. Hwang, H.-Y. Chen, P.-S. Chen, C.-S. Liu, Y. Chi, C.-F. Shu, F.-I. Wu, P.-T. Chou, S.-M. Peng, G.-H. Lee, Inorg. Chem. 44 (2005) 1344.
[63] J. Li, P.I. Djurovich, B.D. Alleyne, M. Yousufuddin, N.N. Ho, J.C. Thomas, J.C. Peters, R. Bau, M.E. Thompson, Inorg. Chem. 44 (2005) 1713.
[64] T. Matsushita, T. Asada, S. Koseki, J. Phys. Chem. C 111 (2007) 6897.
[65] G. Zhou, C.-L. Ho, W.-Y. Wong, Q. Wang, D. Ma, L. Wang, Z. Lin, T.B. Marder, A. Beeby, Adv. Funct. Mater. 18 (2008) 499.
[66] C.-H. Yang, S.-W. Li, Y. Chi, Y.-M. Cheng, Y.-S. Yeh, P.-T. Chou, G.-H. Lee, C.-H. Wang, C.-F. Shu, Inorg. Chem. 44 (2005) 7770.
[67] C.-J. Chang, C.-H. Yang, K. Chen, Y. Chi, C.-F. Shu, M.-L. Ho, Y.-S. Yeh, P.-T. Chou, Dalton Trans. (2007) 1881.
[68] Y. You, K.S. Kim, T.K. Ahn, D. Kim, S.Y. Park, J. Phys. Chem. C 111 (2007) 4052.
[69] Y. You, J. Seo, S.H. Kim, K.S. Kim, T.K. Ahn, D. Kim, S.Y. Park, Inorg. Chem. 47 (2008) 1476.
[70] H.-S. Duan, P.-T. Chou, C.-C. Hsu, J.-Y. Hung, Y. Chi, Inorg. Chem. 48 (2009) 6501.
[71] J.B. Birks, Photophysics of Aromatic Molecules, Wiley-Interscience, London, 1970.
[72] Y. Leydet, D.M. Bassani, G. Jonusauskas, N.D. McClenaghan, J. Am. Chem. Soc. 129 (2007) 8688.
[73] Y.-S. Yeh, Y.-M. Cheng, P.-T. Chou, G.-H. Lee, C.-H. Yang, Y. Chi, C.-F. Shu, C.-H. Wang, ChemPhysChem 7 (2006) 2294.
[74] K. Chen, C.-H. Yang, Y. Chi, C.-S. Liu, C.-H. Chang, C.-C. Chen, C.-C. Wu, M.-W. Chung, Y.-M. Cheng, G.-H. Lee, P.-T. Chou, Chem. Eur. J. 16 (2010) 4315.
[75] C.-C. Cheng, W.-S. Yu, P.-T. Chou, S.-M. Peng, G.-H. Lee, P.-C. Wu, Y.-H. Song, Y. Chi, Chem. Commun. (2003) 2628.
[76] Y.-Y. Chien, K.-T. Wong, P.-T. Chou, Y.-M. Cheng, Chem. Commun. (2002) 2874.
[77] Y.-H. Lin, H.-H. Wu, K.-T. Wong, C.-C. Hsieh, Y.-C. Lin, P.-T. Chou, Org. Lett. 10 (2008) 3211.
[78] C.-H. Fang, Y.-L. Chen, C.-H. Yang, Y. Chi, Y.-S. Yeh, E.Y. Li, Y.-M. Cheng, C.-J. Hsu, P.-T. Chou, C.-T. Chen, Chem. Eur. J. 13 (2007) 2686.
[79] R.J. Watts, S.J. Strickler, J. Chem. Phys. 49 (1968) 3867.

[80] S. Fanni, T.E. Keyes, C.M. O'Connor, H. Hughes, R. Wang, J.G. Vos, Coord. Chem. Rev. 208 (2000) 77.
[81] K. Nozaki, K. Takamori, Y. Nakatsugawa, T. Ohno, Inorg. Chem. 45 (2006) 6161.
[82] C.C. Tong, K.C. Hwang, J. Phys. Chem. C 111 (2007) 3490.
[83] H.-Y. Chen, C.-H. Yang, Y. Chi, Y.-M. Cheng, Y.-S. Yeh, P.-T. Chou, H.-Y. Hsieh, C.-S. Liu, S.-M. Peng, G.-H. Lee, Can. J. Chem. 84 (2006) 309.
[84] T.-C. Lee, J.-Y. Hung, Y. Chi, Y.-M. Cheng, G.-H. Lee, P.-T. Chou, C.-C. Chen, C.-H. Chang, C.-C. Wu, Adv. Funct. Mater. 19 (2009) 2639.
[85] J.A. Treadway, B. Loeb, R. Lopez, P.A. Anderson, F.R. Keene, T.J. Meyer, Inorg. Chem. 35 (1996) 2242.
[86] A.L. Balch, Angew. Chem. Int. Ed. 48 (2009) 2641.